AUTOMATIC SEGMENTATION AND TRACKING OF THROMBUS FORMATION WITHIN IN VITRO MICROSCOPIC VIDEO SEQUENCES

Loic Peter[a], Nicolas Brieu[a], Sjoert Jansen[b,c], Peter A. Smethurst[b,c], Willem H. Ouwehand[b,c,d], Nassir Navab[a]

[a] Computer Aided Medical Procedures, Technische Universitaet Muenchen, Munich, Germany
[b] Department of Haematology, University of Cambridge, Cambridge, United Kingdom
[c] National Health Service Blood and Transplant, Cambridge, United Kingdom
[d] The Wellcome Trust Sanger Institute, Hinxton, United Kingdom

ABSTRACT

There is a need to more accurately link human genetic variance with thrombotic risk. Thrombus formation results from adhesion of blood platelets to a site of injury, followed by their progressive aggregation and occasional embolization. To observe this *in vitro*, blood is perfused over a surface of collagen fibres, during video microscopy. This paper proposes three complementary gradient-based features which, if included in a regularized machine learning framework, yield the accurate segmentation of thrombi during such acquisitions. A novel tracking method of thrombi as deformable growing objects under split and merge conditions is also introduced.

***Index Terms*—** Microscopy image analysis, thrombus formation, segmentation, tracking, supervised classification.

1. INTRODUCTION

Disorders of thrombus formation are a major health issue in developed countries because of their role in the development of coronary artery diseases (CADs). Inappropriate thrombus formation can lead to occlusion of major blood vessels, resulting in myocardial infarction and stroke [1]. The cells most directly involved in thrombus formation are platelets, for which the most widely used test is aggregometry (measuring their clumping in suspension). To study their function, the following setup is used: freshly collected blood is continuously perfused on a surface covered with collagen fibres, leading to the activation and aggregation of platelets which are observed *in vitro* through a microscope/camera system. This provides a complementary approach to the *in vivo* analysis in zebrafish larvae [2] used to confirm the involvement in thrombus formation of novel genes identified in genome-wide association studies. Rapid and efficient methods of data analysis are crucial to conduct large scale studies for the identification of new genetic variants linked to disorders in thrombus formation. A measure of interest is the surface area of the aggregated platelets over time which can be obtained by segmenting and tracking the thrombi.

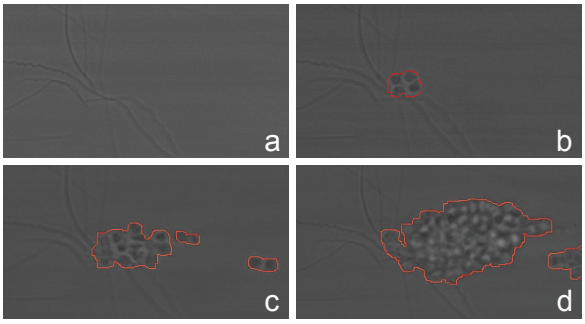


Fig. 1. Example of segmentation results at different times.

The automatic segmentation of the scene is made difficult by the unpredictable and temporally varying texture of the aggregated cells, which excludes in particular a dynamic texture approach as done *in vivo* [2], but also by the deformation of the collagen fibres over time, and by the sudden changes of focus implied by the increase of the blood pressure in the chamber. We develop an approach based on the introduction of new gradient-based features which, if incorporated into a regularized machine learning framework, allows us to deal with these challenges and to achieve accurate and robust segmentation. We also introduce an innovative and adapted scheme for linking the individual thrombi over time.

The increasing amount of image data in cellular biology has motivated the development of algorithms for automatic microscopy image analysis. The detection and segmentation of single cells has been widely studied using different mathematical approaches, in particular gradient-based features [3, 4] and statistical learning [5]. Segmentation of cells inside a cluster [6] is a topic of increasing interest and closer to our purpose. Previous methods however require a minimal amount of structure in the cellular cluster, which is not observed in our application (cf. Fig. 1). Also, the changes of texture in time exclude methods relying strongly on texture identification. We propose in this paper a combination of gradient-based features able to deal with this high variability.

2. METHODS

We introduce in this section our algorithm for the automatic detection and tracking of structured and unstructured thrombi. We introduce our gradient-related features and their use for the segmentation of the thrombi in section 2.1. We then present our strategy to track the merging and the splitting of individual thrombi over time in section 2.2.

2.1. Segmentation

For each pixel location $\mathbf{x}_0 = (x_0, y_0)$, we define the circular strength (2.1.1), the orientation homogeneity (2.1.2), and the minimum directional magnitude average (2.1.3) of the gradient vectors in a centered disk-shaped neighbourhood $D^\rho_{\mathbf{x}_0}$ of radius ρ. Based on these features, pixels are classified using supervised classification algorithms (2.1.4).

2.1.1. Circular Strength

The thrombus can take two different appearances, well-defined platelets or chaotic thrombus, which are characterized by circularly and randomly distributed gradients of high magnitude respectively. From this observation, we define the *circular strength* at the pixel location $\mathbf{x_0}$ as follows

$$\begin{aligned} f^\rho_{\mathrm{CS}}(\mathbf{x}_0) &= \sum_{\mathbf{x}\in D^\rho_{\mathbf{x}_0}} \frac{\left\langle \overrightarrow{\nabla I}(\mathbf{x}) | \overrightarrow{u}_{\mathbf{x}_0}(\mathbf{x}) \right\rangle^2}{N_\nabla(\mathbf{x})} \\ &= \sum_{\mathbf{x}\in D^\rho_{\mathbf{x}_0}} N_\nabla(\mathbf{x})\ \cos^2(\alpha_{\mathbf{x}_0}(\mathbf{x}) - \theta_\nabla(\mathbf{x})) \end{aligned} \tag{1}$$

where $\langle|\rangle$ denotes the scalar product operator, $\overrightarrow{u}_{\mathbf{x}_0}(\mathbf{x})$ and $\alpha_{\mathbf{x}_0}(\mathbf{x})$ are the unit polar vector and the polar angle at $\mathbf{x}$ respectively in the polar coordinate system of pole $\mathbf{x}_0$, and $N_\nabla(\mathbf{x})$ and $\theta_\nabla(\mathbf{x})$ are the magnitude and the direction of the gradient at the pixel location $\mathbf{x}$. This feature is of particular interest in our application. It has low values in areas where the gradients have a low magnitude e.g homogeneous background. In well-defined platelets, the circular repartition of the gradients results in $\cos^2(\alpha_{\mathbf{x}_0}(\mathbf{x}) - \theta_\nabla(\mathbf{x})) \approx 1$ for any $\mathbf{x} \in D^\rho_{\mathbf{x}_0}$. The gradient magnitudes are therefore preserved. In fibres and unstructured thrombus regions, gradients are oriented perpendicularly to the fibre and randomly respectively. This results in an attenuation of the gradient magnitudes. As shown in Fig. 2 (3), the circular strength is characterized by lower values in the homogeneous background (a) and in the fibres (b)-(c) than in the well-defined (d) and unstructured (e) thrombus. However, the fibres are only partially attenuated and could therefore still disrupt the classification results if they display high gradient magnitudes. This is solved by the introduction in section 2.1.2 and 2.1.3 of two additional gradient-based features.

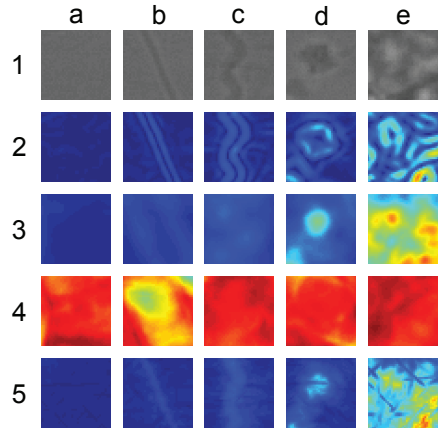


Fig. 2. Response of our features in typical objects. Horizontally: homogeneous background (a), straight fibre (b), locally circular fibre (c), well-defined platelet (d), chaotic thrombus (e). Vertically: raw image (1), gradient magnitude (2), circular strength (3), orientation homogeneity (4), minimum directional magnitude average (5).

2.1.2. Orientation Homogeneity

The second feature is inspired by the work of Dalal and Triggs [7] and based on a normalized histogram of gradients orientation over $D^\rho_{\mathbf{x}_0}$ which we weight by the gradient magnitudes to lower the influence of noise-related gradients. The p^{th} bin of the histogram reads as

$$h^\rho_p(\mathbf{x}_0) = \frac{\sum_{\mathbf{x}\in D^\rho_{\mathbf{x}_0}} N_\nabla(\mathbf{x})\ \mathbf{1}_{[(p-1)\frac{2\pi}{P};p\frac{2\pi}{P}[}(\theta_\nabla(\mathbf{x}))}{\sum_{\mathbf{x}\in D^\rho_{\mathbf{x}_0}} N_\nabla(\mathbf{x})}, \tag{2}$$

where P is the number of bins. We characterize the structure of the obtained histogram using the Shannon entropy. This defines our *orientation homogeneity* measure

$$f^\rho_{\mathrm{OH}}(\mathbf{x}_0) = \sum_{p=1}^{P} h_p(\mathbf{x}_0) \log h_p(\mathbf{x}_0), \tag{3}$$

which has low values in objects presenting preferential directions, e.g. in collagen fibres, and high values in regions where all the directions are equally represented, e.g. in the thrombus and in the homogeneous background because of the circularity (well-defined platelet) or the randomness of the gradient directions (chaotic thrombus and homogeneous background). The response to this second feature is displayed in Fig. 2 (4).

2.1.3. Minimum Directional Magnitude Average

In some particular case, the collagen fibres locally exhibit circular patterns. This is displayed in Fig. 2 (c). At the centers of these circular shapes, the two previous features give a high response. Inspired by the Ray features [4] in the context of isolated cell detection, we introduce a third feature as follows.

K equally spaced lines of equal length ρ and of directions $(\theta_k)_{1\leq k\leq K}$ are drawn starting from $\mathbf{x}_0$. We compute for each direction θ_k the mean $M_k^\rho(\mathbf{x}_0)$ of the gradient magnitude along this line. We then define our third feature as the minimum of these averages, $f_{\text{MD}}^\rho(\mathbf{x}_0) = \min_{1\leq k\leq K} M_k^\rho(\mathbf{x}_0)$. This obtained feature is low next to the fibres since there exists always a direction of escape along which no object boundary is met, and high in well-defined platelets and chaotic thrombus since these objects are surrounded by gradients of high magnitude in every direction. This feature completes the circular strength by offering a better convervation of edges. The response to this feature is displayed in Fig. 2 (5).

2.1.4. Supervised Classification

We include the three aforementioned gradient-based features, taken at different scales ρ (from 8 to 20 pixels), in two different supervised classification algorithms, Adaboost [8] and Decision tree [9]. We also incorporate temporal information by including a binary feature stating the classification result at the previous frame. One video is arbitrarily chosen and dedicated to the learning step. More precisely, the learning base is generated by randomly drawing points within the learning video in both background and thrombus areas. We checked the robustness of the results to this initial random drawing and permutations of the learning videos have been tried without noticing any significant change of performance. To avoid overfitting of the classifiers to the learning examples, we crop our final classifiers by performing pruning (resp. reducing the number of iterations) on the decision tree (resp. Adaboost classifier). We investigate the use of post-processing methods to suppress possible false detection as follows. Since the output of the decision tree is binary, we perform a series of morphological operations (opening, suppression of small objects, suppression of small holes) to obtain the final result. The output of AdaBoost can be expressed as a probability function [10]. The segmentation is obtained, in this case, by introducing the fixed probability functions into a region-based level-set framework [11]. The parameters of this regularization step are experimentally set to optimize the performance.

2.2. Tracking

The detection of platelets *vs* background regions in each frame opens the way to the computation of the overall area of aggregation over time. It is, however, crucial for a more precise study of thrombus formation to also derive the individual tracks of the thrombi and to detect their possible merging and splitting. This section proposes an original approach to this problem. Based on the observations that the thrombi are not constantly textured over time and that their movement is limited by their attachment to the collagen fibres, we develop a nearest-neighbour method relying only on their position and shape. Their possible deformation, splitting, and merging make the tracking of the thrombi intrinsically ill-posed.

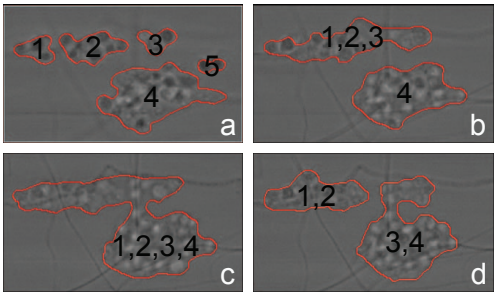


Fig. 3. Example sequence of frames for the tracking of thrombi. (a)-(b) Thrombi T_1, T_2, T_3 merge into $T_{1,2,3}$ while T_5 disappears. (b)-(c) Thrombus $T_{1,2,3}$ and T_4 merge into $T_{1,2,3,4}$. (c)-(d) Thrombus $T_{1,2,3,4}$ splits into $T_{1,2}$ and $T_{3,4}$.

Let us consider a thrombus T at a given time t and assume that it has been accurately tracked until then. The history of this thrombus is represented by the collection of detections $(\mathcal{O}_i^T)_{1\leq i\leq t}$ at previous times. We set $\mathcal{O}_i^T = \emptyset$ in the frames where the thrombus T is absent. We then characterize the thrombus T at time t by the area of maximal thrombus presence at previous times, i.e. by $\Omega_T(t) = \text{argmax}_{\mathbf{x}} \left[\sum_{i\leq t} \mathbf{1}_{\mathcal{O}_{T,i}}(\mathbf{x})\right]$. We then define the distance between the thrombus T and a binary object $\mathcal{O}$ by

$$d(\Omega_T(t), \mathcal{O}) = \frac{1}{|\Omega_T(t)|} \sum_{\mathbf{x}\in\Omega_T(t)} \min_{\mathbf{y}\in\mathcal{O}} \|\mathbf{x}-\mathbf{y}\|_2 \qquad (4)$$

We would like to find at time $t+1$ which of the N objects $(\mathcal{O}_i)_{1\leq i\leq N}$ detected at this time corresponds to the thrombus T. We then define the cost of associating the thrombus T to the object $\mathcal{O}_i$ directly as the distance $d(\Omega_T(t), \mathcal{O}_i)$ defined by Eq. (4). From the observation that single platelets are more likely to disappear than big agglomerated thrombi, we define the cost of disappearance as proportional to the size of the thrombus at time t. The balance between the distance-related cost and the size-related cost is experimentally set. In a final step, each thrombus is linked to the object, including the empty set, which has the lowest association cost.

Our approach has until now considered each thrombus independently by associating it to its nearest object in the next frame. We introduce dependence between the decision of associations by incorporating an additional constraint on the size of the merged thrombi as follows. Let us assume that, after the computation of the association costs, several thrombi are supposed to merge into the same object $\mathcal{O}$. Our size constraint consists in checking if the summed sizes of these initial thrombi exceed the size of $\mathcal{O}$. If this is the case, we select the thrombus for which the initial cost was the highest among all the thrombi merging into $\mathcal{O}$ and assign it to its second choice. We iterate over all the assignments as long as the size constraint is not satisfied for all merging thrombi.

Video	Decision Tree		Adaboost		Tracking
	Dc	Ppv	Dc	Ppv	Pna
#1	0.92	0.89	0.90	0.84	0.97
#2	0.87	0.95	0.86	0.93	0.93
#3	0.87	0.98	0.85	0.96	0.87
#4	0.88	0.92	0.85	0.88	0.99
Mean	**0.89** $\pm$**0.02**	**0.94** $\pm$**0.04**	**0.87** $\pm$**0.02**	**0.90** $\pm$**0.05**	**0.94** $\pm$**0.05**

Table 1. Quantitative validation of our methods.

3. RESULTS

We qualitatively and quantitatively evaluate our segmentation method on five *in vitro* microscopic video sequences, recorded with a Evos fl phase-contrast microscope. As aforementioned, one video is used for learning. Ground-truths are manually delineated by a trained biologist and accuracy is measured using the Dice coefficient (Dc) and the positive predicted value (Ppv). The tracking performance is measured using the proportion of thrombi which are correctly tracked all along the video (Pna), excluding the ambiguous cases for a human observer which represent less than 7% of the thrombi within the data set. The quantitative results are shown in Table 1. The decision-tree performs similarly or better on all the videos, which can be explained by the complementary nature of our features. The relevance of the features depends on the object on which we apply the classification, and decision trees have the advantage to adapt the classifier to each pixel in function of the response at the first nodes, whereas AdaBoost classifiers are the same for every pixel. Qualitative results are presented in Fig. 1 for the segmentation problem and in Fig. 4 for the tracking problem. We observe the ability of our approach to accuratly detect merging and splitting of thrombi. This leads to the possible assessment of embolization, i.e. of the detachment of thrombus in downstream blood circulation.

4. CONCLUSION

We proposed in this paper a set of three complementary gradient-based features to separate background from thrombus. They were included in a decision-tree framework and provided an accurate segmentation despite a high variability within the desired objects. More generally, this set of features could provide new tools for any segmentation of isotropically contrasted objects among a background filled by curvilinear structures. A well-chosen definition of thrombus and distances between thrombi and objects allowed the successful application of an adapted nearest-neighbour tracking approach.

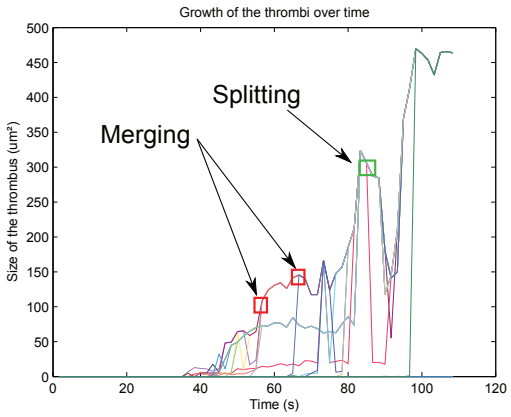


Fig. 4. Growth of individual thrombi on an example video. Each colored curve represents the size of an individual thrombus over time. The video was spatially cropped to reduce the number of thrombus and improve the lisibility. A better representation remains to be found as future work.

5. REFERENCES

[1] Giovanni Dav and Carlo Patrono, "Platelet activation and atherothrombosis," *New England Journal of Medicine*, vol. 357, no. 24, pp. 2482–2494, 2007.

[2] N. Brieu, M. Groher, J. Serbanovic-Canic, A. Cvejic, W. Ouwehand, and N. Navab, "Joint thrombus and vessel segmentation using dynamic texture likelihoods and shape prior," in *MICCAI*, 2011, vol. 6893, pp. 579–586.

[3] T. Liu, G. Li, J. Nie, A. Tarokh, X. Zhou, L. Guo, J. Malicki, W. Xia, and S. Wong, "An automated method for cell detection in zebrafish," *Neuroinformatics*, vol. 6, pp. 5–21, 2008.

[4] K. Smith, A. Carleton, and V. Lepetit, "Fast ray features for learning irregular shapes," in *CVPR*, 2009, pp. 397 –404.

[5] S. Mohapatra and D. Patra, "Automated cell nucleus segmentation and acute leukemia detection in blood microscopic images," in *ICSMB*, 2010, pp. 49 –54.

[6] J. Pan, T. Kanade, and M. Chen, "Heterogeneous conditional random field: Realizing joint detection and segmentation of cell regions in microscopic images.," in *CVPR*, 2010, pp. 2940–2947.

[7] N. Dalal and B. Triggs, "Histograms of oriented gradients for human detection," in *CVPR*, 2005, pp. 886–893.

[8] Y. Freund and R. E. Schapire, "A decision-theoretic generalization of on-line learning and an application to boosting," *Journal of Computer and System Sciences*, vol. 55, no. 1, pp. 119–139, August 1997.

[9] L. Breiman, J. Friedman, C. J. Stone, and R. A. Olshen, *Classification and Regression Trees*, Chapman and Hall/CRC, 1984.

[10] J. Friedman, T. Hastie, and R. Tibshirani, "Additive logistic regression: A statistical view of boosting," *The Annals of Statistics*, vol. 28, no. 2, pp. 337–407, 2000.

[11] N. Paragios and R. Deriche, "Geodesic active regions for supervised texture segmentation," in *ICCV*, 1999, pp. 926–932.